REFERENCES AND NOTES

1. H. Matsushita *et al.*, *Nature* **482**, 400–404 (2012).
2. N. A. Rizvi *et al.*, *Science* **348**, 124–128 (2015).
3. J. C. Castle *et al.*, *Cancer Res.* **72**, 1081–1091 (2012).
4. A. Snyder *et al.*, *N. Engl. J. Med.* **371**, 2189–2199 (2014).
5. P. F. Robbins *et al.*, *Nat. Med.* **19**, 747–752 (2013).
6. T. N. Schumacher, R. D. Schreiber, *Science* **348**, 69–74 (2015).
7. M. Greaves, *Cancer Discovery* **5**, 806–820 (2015).
8. E. C. de Bruin *et al.*, *Science* **346**, 251–256 (2014).
9. M. Jamal-Hanjani *et al.*, *Ann. Oncol.* mdw037 (2016).
10. M. S. Lawrence *et al.*, *Nature* **505**, 495–501 (2014).
11. M. S. Rooney, S. A. Shukla, C. J. Wu, G. Getz, N. Hacohen, *Cell* **160**, 48–61 (2015).
12. S. A. Shukla *et al.*, *Nat. Biotechnol.* **33**, 1152–1158 (2015).
13. Materials and methods are available as supplementary materials on *Science* Online.
14. L. T. Nguyen, P. S. Ohashi, *Nat. Rev. Immunol.* **15**, 45–56 (2015).
15. S. R. Hadrup *et al.*, *Nat. Methods* **6**, 520–526 (2009).
16. S. Read, V. Malmström, F. Powrie, *J. Exp. Med.* **192**, 295–302 (2000).
17. E. M. Van Allen *et al.*, *Science* **350**, 207–211 (2015).
18. L. B. Alexandrov *et al.*, *Nature* **500**, 415–421 (2013).
19. B. E. Johnson *et al.*, *Science* **343**, 189–193 (2014).
20. T. A. Yap, M. Gerlinger, P. A. Futreal, L. Pusztai, C. Swanton, *Sci. Transl. Med.* **4**, 127ps10 (2012).
21. J. Zhang *et al.*, *Science* **346**, 256–259 (2014).

ACKNOWLEDGMENTS

C.S. is a senior Cancer Research UK (CRUK) clinical research fellow and is funded by CRUK (TRACERx), the CRUK Lung Cancer Centre of Excellence, Stand Up 2 Cancer Laura Ziskin prize (SU2C), the Rosetrees Trust, NovoNordisk Foundation (ID 16584), the Prostate Cancer Foundation, the Breast Cancer Research Foundation, the European Research Council (THESEUS), and EU FP7 (PREDICT). S.A.Q is funded by a CRUK Career Development Fellowship, CRUK Biotherapeutic Programme Grant, World Wide Cancer Research, and a Cancer Research Institute Investigator Award. A.J.S.F receives support from the Sam Keen Foundation. R.R., N.M., N.J.B., and G.A.W. are funded by the TRACERx CRUK grant. T.B.K.W. is funded by the FP7-People-2013-ITN [grant (2013)607722 – PloidyNet]. C.T.H. is funded by the Rosetrees Trust. C.J.W. is a Scholar of the Leukemia and Lymphoma Society and acknowledges support from the Blavatnik Family Foundation, NIH/National Heart, Lung, and Blood Institute (grant 1R01CA155010-02) and NIH/National Cancer Institute (grants 1R01CA182461-01 and 1R01CA184922-01). S.S. is funded by the Cancer Research UK–UCL Centre, and M.J.H. is funded by a CRUK-UCL Centre Clinical Research Fellowship. A.A. is funded by the Cancer Research UK–UCL Centre Cancer Immuno-Therapy Accelerator Award. We thank N. Hacohen and S. Turajlic for helpful advice on the manuscript. This research is supported by the National Institute for Health Research, the University College London Hospitals Biomedical Research Centre, and the Cancer Research UK University College London Experimental Cancer Medicine Centre. Certain data were received under a material transfer agreement with Memorial Sloan Kettering Cancer Center. Data from multiregion sequenced NSCLC are available at the European Bioinformatics Institute (accession no. EGAS00001000809). Data from the Rizvi cohort (*2*) are available at the database of Genotypes and Phenotypes (dbGAP) (accession no. phs000980.v1.p1). Data from the Snyder cohort (*4*) are available at dbGAP (accession no. phs001041.v1.p1). Data from the Van Allen cohort (*17*) are available at dbGAP (accession no. phs000452.v2.p1). The results published here are in part based on data generated by a TCGA pilot project established by the National Cancer Institute and National Human Genome Research Institute. The data were retrieved through dbGaP authorization (accession no. phs000178.v9.p8). Information about TCGA and the investigators and institutions that constitute the TCGA research network can be found at http://cancergenome.nih.gov. C.S. is a paid advisor for Janssen, Boerhinger Ingelheim, Ventana, Novartis, Roche, Sequenom, Natera, Grail, Apogen Biotechnologies, Epic Biosciences, and the Sarah Cannon Research Institute. D.S. is a paid advisor for Bristol-Myers Squibb, Roche, Novartis, Merck, and Amgen. B.S. is a paid advisor for Bristol-Myers Squibb. T.A.C. is a cofounder of and holds equity in Gritstone Oncology; is a paid advisor for Geneocea, OncoSpire, and Cancer Genetics; and receives funding from Bristol-Myers Squibb for research on the genomics of immune response. N.A.R. is a cofounder of and holds equity in Gritstone Oncology. E.M.V.A. is a paid advisor for Syapse, Roche Ventana, Takeda, and Third Rock Ventures. M.D.H is a paid advisor for Bristol-Myers Squibb, Merck, Genentech, AstraZeneca, and Neon. J.D.W is a paid advisor for Bristol-Myers Squibb. L.A.G. is a paid scientific advisor for Novartis, Boehringer Ingelheim, Foundation Medicine, and Warp Drive Bio. C.S., N.M., R.R., S.A.Q., and K.S.P. are co-inventors on UK patent applications (1516047.6, 1601098.5, 1601098.5, and 1601099.3) filed by Cancer Research Technology relating to methods for identifying and targeting neoantigens, methods of predicting prognosis of cancer patients, and/or identifying cancer patients who will benefit from treatment that involves determining the number of neoantigens.

SUPPLEMENTARY MATERIALS

www.sciencemag.org/content/351/6280/1463/suppl/DC1
Materials and Methods
Figs. S1 to S7
Tables S1 to S5
References (*22*–*38*)

15 August 2015; accepted 11 February 2016
Published online 3 March 2016
10.1126/science.aaf1490

TRANSPORTER FUNCTION

Direct observation of proton pumping by a eukaryotic P-type ATPase

Salome Veshaguri,[1,2,3,4] Sune M. Christensen,[1,2,3,4]* Gerdi C. Kemmer,[5] Garima Ghale,[1,2,3,4] Mads P. Møller,[1,2,3,4] Christina Lohr,[1,2,3,4] Andreas L. Christensen,[1,2,3,4] Bo H. Justesen,[5] Ida L. Jørgensen,[5] Jürgen Schiller,[6] Nikos S. Hatzakis,[1,2,3,4] Michael Grabe,[7] Thomas Günther Pomorski,[5] Dimitrios Stamou[1,2,3,4]†

In eukaryotes, P-type adenosine triphosphatases (ATPases) generate the plasma membrane potential and drive secondary transport systems; however, despite their importance, their regulation remains poorly understood. We monitored at the single-molecule level the activity of the prototypic proton-pumping P-type ATPase *Arabidopsis thaliana* isoform 2 (AHA2). Our measurements, combined with a physical nonequilibrium model of vesicle acidification, revealed that pumping is stochastically interrupted by long-lived (~100 seconds) inactive or leaky states. Allosteric regulation by pH gradients modulated the switch between these states but not the pumping or leakage rates. The autoinhibitory regulatory domain of AHA2 reduced the intrinsic pumping rates but increased the dwell time in the active pumping state. We anticipate that similar functional dynamics underlie the operation and regulation of many other active transporters.

Electrochemical gradients across cellular membranes control many essential biological processes. These gradients are generated by primary active transporters and are used to drive the exchange of other solutes through secondary active transporters and to facilitate signaling through ion channels (*1*). Patch clamp recording has made it possible to observe the functional dynamics of single ion channels, revealing discrete on and off states, subconductance states, and other mechanistically important features that macroscopic experiments cannot probe (*2*). However, despite extensive structural and biochemical efforts (*3*), we currently lack a similar depth of understanding of transporters, because they in general do not produce electrically detectable single-molecule transport signals (*4*–*8*). We monitored at the single-molecule level the functional dynamics of a eukaryotic primary active transporter, *Arabidopsis thaliana* H^+–adenosine triphosphatase (ATPase) isoform 2 (AHA2, referred to as the proton pump), which is responsible for energizing the plasma membrane of plants and fungi (figs. S1 and S2) (*3*, *9*). This provided insights into how the activity of P-type ATPases is modulated by autoregulatory terminal domains (R domains) and pH gradients (*10*, *11*).

We used total internal reflection fluorescence (TIRF) microscopy to image with high throughput single nanoscopic lipid vesicles tethered to a solid support (Fig. 1, A and B, and figs. S3 and S4). Tethering was accomplished with a biotin/neutravidin protocol (*12*), which maintains the native function and diffusivity of reconstituted transmembrane proteins (*13*) and the vesicles' spherical morphology (*14*) and low passive ion permeability (*15*). The fluorescence intensity of all single vesicles was quantitatively converted to pH (fig. S5) and tracked over periods of up to 30 min.

Initial studies were carried out on the well-studied activated form of AHA2, which lacks the

[1]Bionanotecnology and Nanomedicine Laboratory, University of Copenhagen, Copenhagen, Denmark. [2]Department of Chemistry, University of Copenhagen, Copenhagen, Denmark. [3]Nano-Science Center, University of Copenhagen, Copenhagen, Denmark. [4]Lundbeck Foundation Center Biomembranes in Nanomedicine, University of Copenhagen, Copenhagen, Denmark. [5]Centre for Membrane Pumps in Cells and Disease - PUMPKIN, Department of Plant and Environmental Sciences, University of Copenhagen, Frederiksberg, Denmark. [6]Institute of Medical Physics and Biophysics, Faculty of Medicine, University of Leipzig, Leipzig, Germany. [7]Cardiovascular Research Institute, Department of Pharmaceutical Chemistry, University of California, San Francisco, CA 94143, USA.
*Present address: Novozymes A/S, 2880 Bagsvaerd, Denmark.
†Corresponding author. E-mail: stamou@nano.ku.dk

flexible C-terminal autoinhibitory R domain ($AHA2^R$) (Fig. 1A and figs. S1 to S3) (*9*). Initialization of H^+ pumping into the vesicle lumen was triggered by the addition of ATP and Mg^{2+}, which are non–membrane-permeable and thus only activate proton pumps with an outward-facing ATP-binding domain (Fig. 1A) (*12*). Consistent with this, we never observed lumenal alkalinization (Fig. 1C). Acidification kinetics reached a plateau of well-defined pH (ΔpH_{max}) as a result of a dynamic steady state, in which active pumping (influx) of protons matched the passive leakage (efflux) of protons through the membrane due to the buildup of a proton motive force (*16*). As expected, addition of the protonophore CCCP collapsed the H^+ gradients (Fig. 1C), whereas controls performed without Mg^{2+}, ATP, or $AHA2^R$ showed no response (fig. S6D). Furthermore, the activity of the pump was blocked by the addition of the specific inhibitor vanadate (*11*), and it decayed after ATP and Mg^{2+} were flushed out (fig. S7). To control for potential artifacts arising from the surface tethering of vesicles, we performed a side-by-side comparison with vesicles suspended in solution, which proved indistinguishable within experimental uncertainties (Fig. 1C and fig. S6). Taken together, these results demonstrate that we were able to observe the $AHA2^R$-mediated and ATP-fueled pumping of protons against their concentration gradient into the lumen of single vesicles. The single-vesicle experiments revealed a heterogeneity of acidification rates and ΔpH_{max} values between vesicles (Fig. 1C) that remain masked in the ensemble averages (*16*).

At the low protein-to-lipid molar ratio (1:12,000) used in our experiments, 84% of vesicles exhibited no detectable pH changes (Fig. 1C and Fig. 2A, top trace) indicating the absence of active pumps and thus suggesting that there are only a few active pumps in each of the remaining vesicles whose pH changed over time (hereafter termed active vesicles). We inspected the pH changes in the 16% of active vesicles and indeed found that all of them exhibited the hallmark of single-molecule behavior; i.e., stochastic changes between discrete states (Fig. 2A). Because the passive leakage rates of the vesicles are constant over time (fig. S10), these data demonstrate that the individual proton pumps are stochastically transitioning between active and inactive states. This behavior is termed functional dynamics (*17*–*24*) and is key to the function and regulation of ion channels (*25*).

Further examination of all active vesicle traces revealed that ~60% of them reverted back to the zero ΔpH baseline after switching off, strongly suggesting the presence of only one molecule, because it is improbable for many molecules to switch off simultaneously (Fig. 2A). In the remaining traces (~40%), we observed two or three discrete plateaus, a feature that has been observed in all studies of single channels to date and has been interpreted to demonstrate that the activity of multiple single molecules can be discretely resolved. The latter conclusion was further supported by experiments in which titration of the protein–to-lipid ratio modulated the percentage of multiple plateaus (fig. S5G), excluding the possibility that multiple plateaus represent multiple single-molecule activity states. These observations allowed us to unambiguously identify the traces resulting from a single active proton pump, which we then selected for further analysis. The activity of single proton pumps was amplified and reported by ~10^3 pH-sensitive fluorophores (figs. S3 and S4) (*16*), circumventing the issue of photobleaching that fundamentally restricts most fluorescence studies of single molecules.

Dynamic transitions between active and inactive states were also observed in experiments with wild-type AHA2 (Fig. 2C), demonstrating that they are not solely a property of the truncated version. Here ~80% of all vesicles were inactive, whereas ~73% of those that showed activity had a single plateau indicating a single molecule (Fig. 2D). With wild-type AHA2, we succeeded in using a SNAP-tag to fluorescently label the protein and count directly the number of proteins per vesicle (Fig. 2E). This allowed us to observe activity dynamics and directly count the number of labeled proteins at the same time on the same vesicles (Fig. 2C and 2E). We then estimated the labeling efficiency and the probability that a proton pump was active (*12*). We were thus able to quantitatively convert the bleach-step distribution to a distribution of active molecules per vesicle and demonstrated that 70 ± 15% of active proteoliposomes carried one active molecule (Fig. 2F). This was in quantitative agreement with the distribution of activity plateaus (~73%) (Fig. 2D), providing an additional demonstration that we can resolve and record the functional dynamics of the proton pump at the single-molecule level.

The activity of the proton pump, and probably other active transporters, is thus not constant in time (Fig. 2). Therefore, for transporters (just like ion channels), the rates measured in macroscopic experiments are the product of the active-state probability and the intrinsic pumping rate. To quantitatively analyze the kinetics and dynamics of pumping, we constructed a physical model of a single vesicle (*12*), which accounts for several parameters that affect the acidification kinetics, including passive and active ionic fluxes across

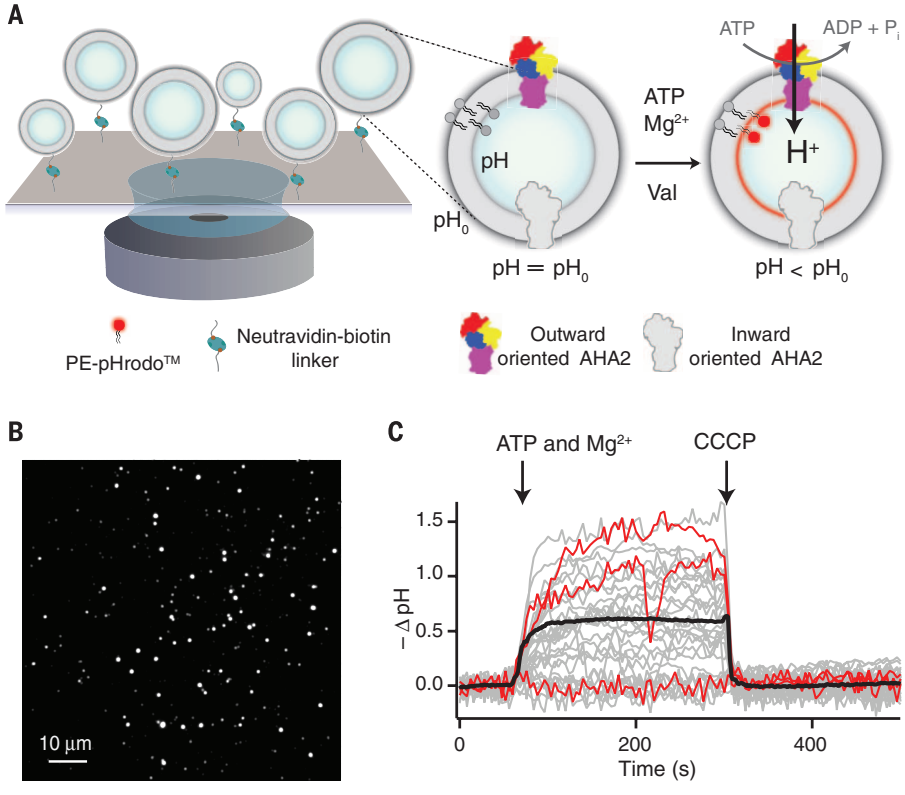

Fig. 1. Imaging proton pumping into the lumen of single surface-tethered vesicles using TIRF microscopy. (**A**) Illustration of AHA2 reconstituted vesicles tethered to a passivated glass surface and imaged on and individual basis with TIRF microscopy. Zoom: Extravesicular addition of both ATP and Mg^{2+} activated exclusively outward-facing AHA2 molecules, triggering H^+ pumping in the vesicle lumen. We quantified changes in the vesicular H^+ concentration by calibrating the response of the lipid-conjugated pH-sensitive fluorophore pHrodo. Valinomycin was always present to mediate K^+/H^+ exchange and prevent the buildup of a transmembrane electrical potential. (**B**) TIRF image of single vesicles tethered on a passivated glass slide. (**C**) Acidification kinetics of single vesicles upon addition of ATP and Mg^{2+}. Red traces highlight three representative signals from single vesicles, showcasing the absence of transport activity, the continuous pumping of protons, and fluctuations in proton-transport activity. The black trace is the average of ≈600 single-vesicle traces. As expected, addition of the protonophore CCCP collapsed the proton gradient established by $AHA2^R$.

the membrane, proton buffering in the lumen, vesicle size, and buildup of membrane potential (Fig. 3A) (*26*). Proton pumping is modeled with a fixed rate (I_P), a lifetime (t_{on}), and time between pumping events (t_{off}) Fig. 3, A and B. The vesicle is assumed to have a passive membrane permeability to protons (P_{leak}), which is constant over time, as revealed by control experiments (fig. S10). The stochastic switching of the pump between active and inactive states was extracted directly from the traces and used as time-dependent input to the model. The model is constrained to fit the entire trace, and it provides a realistic description of the full electrochemical gradient and a direct estimation of the absolute numbers of pumped and leaked ions.

Initially, all experimental traces were fit with the model by varying two parameters: I_P and P_{leak}. This provided a good quantitative description of the majority of AHA2^R traces (~65% of 126 counts, fig. S8); however, it systematically underestimated the observed leaking rates for the remaining traces (Fig. 3B, blue line), suggesting the existence of an additional proton-leaking route apart from passive leakage through the membrane (fig. S8). Indeed, leakage of ions through transporters has been reported before; e.g., for P- and V-type ATPases (*27*, *28*). To test this hypothesis, we collected all lifetimes of exponential fits to the leakage kinetics from traces transitioning between active and inactive states. The histogram of leakage lifetimes (fig. S9C) had two clearly separated peaks: one that according to control experiments corresponded to passive leakage through the membrane (a transmembrane leak) and another that was approximately 20 times faster (figs. S9 and S10). The latter peak was specifically inhibited by the addition of vanadate, which locked the pump in the E2 state (*11*) (fig. S9D), demonstrating that the leak is not passively mediated by the membrane (or the protein/membrane interface) but by the pump itself. Because vanadate is membrane-impermeable, we can exclude the possibility that the fast-leak component originated from pumps with the opposite orientation, because they would not be blocked by vanadate. We thus modified the model to include a time-dependent transprotein proton leak (P_{AHA2}), which turns on once pumping stops and turns off at the beginning of the next pumping cycle (Fig. 3C, blue dotted line). As expected, the revised model considerably improved the fits of the remaining traces (Fig. 3B, red line, and fig. S8).

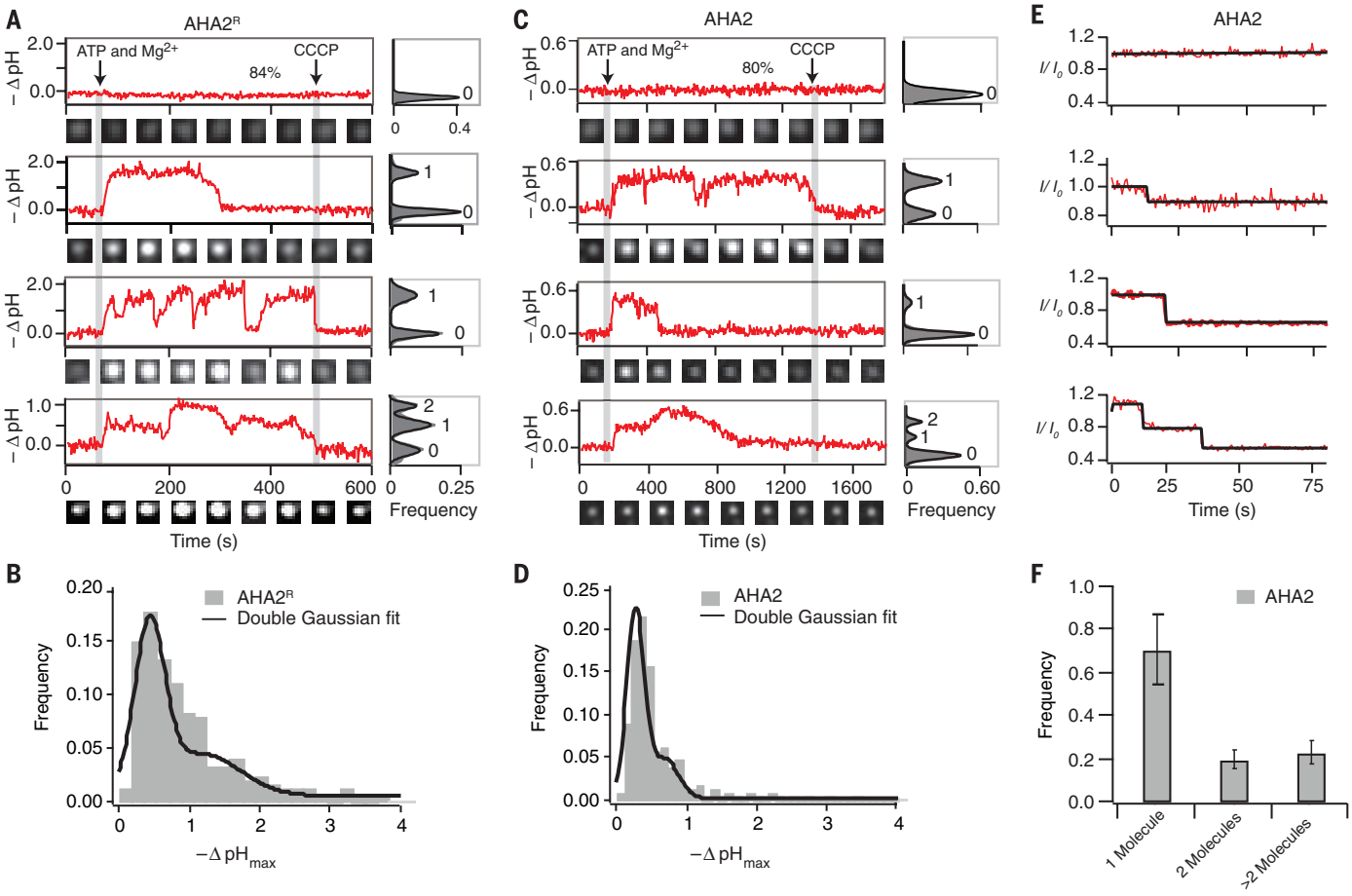

Fig. 2. Single-molecule observation of proton pumping reveals active and inactive states. (**A**) Typical examples of pH changes inside individual AHA2^R reconstituted vesicles. ATP and Mg^{2+} (2 mM) were added to initiate proton pumping, and CCCP (5 μM) was added to collapse the pH gradients. Traces show −ΔpH defined as a difference between the initial and final pH. Images of each respective liposome at different time points are shown below each trace. At the right-hand side of the traces, we plotted histograms of pH plateaus numbered to indicate the number of active pumps per vesicle. The pH inside the majority of vesicles showed no changes indicating the absence of functional transporter molecules (top panel). For the majority of active vesicles, we observed intermittent H^+ pumping, indicating the presence of single molecules (middle panels). The observation of two discrete steady-state pH plateaus in single-vesicle traces indicated the occasional presence of two active pumps per single vesicle (bottom panel). (**B**) Population histogram of pH plateaus for AHA2^R-reconstituted vesicles (n = 3, where hereafter n is the number of independent experiments). (**C** and **D**) Same as in (A) and (B) but for full-length AHA2. For (D), n = 2. Labeling of AHA2 with Alexa Fluor 647 enabled counting on the same vesicles of both the number of labeled AHA2 proteins (**E**) and of the respective activity dynamics (C). (**F**) The histogram of active proteins per vesicle was calculated from step-bleaching analysis of the data in (E) that was corrected for labeling efficiency and the probability that a proton pump is active (*12*). The two independent methods for estimating the number of active molecules agreed that ~70% of vesicles containing a protein have one active proton pump.

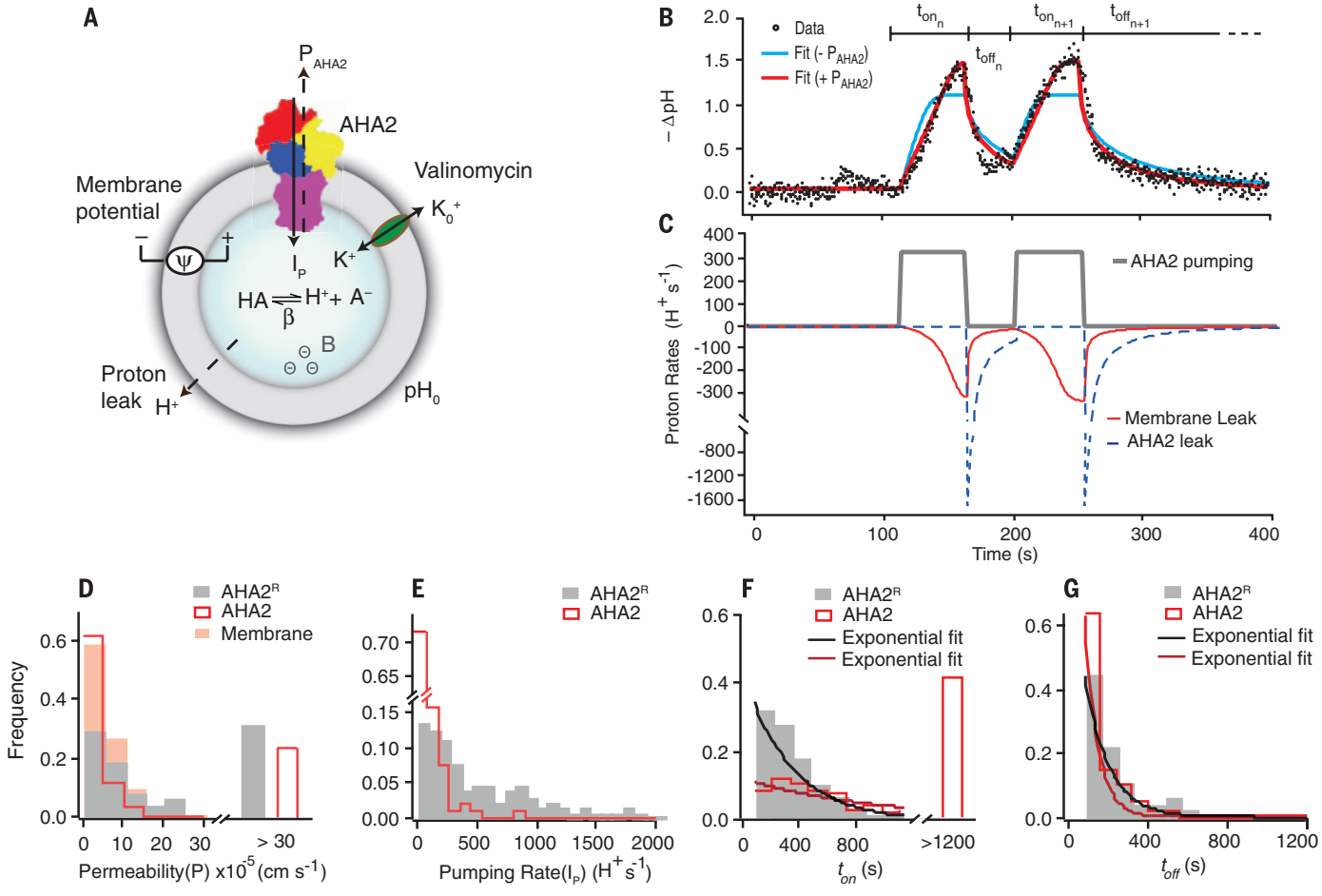

Fig. 3. Modeling active, inactive, and leaky states and their role in auto-inhibiting proton pumps. (**A**) The main parameters of the physical model we used to fit changes in the vesicular pH were pumping rate (I_p), protein-associated leak (P_{AHA2}), membrane leak (P_{leak}), valinomycin-induced K^+ permeability (P_{K+}), buffering capacity in the interior of the vesicle (β), and electrical potential across the membrane (Ψ) (*12*). (**B**) Example of a typical proton pumping trace and respective fits without (blue) and with (red) a transprotein proton leak. A threshold in the first derivative of the pH kinetics (*12*) was used to define the lifetime of the active state t_{on} and the time between pumping events t_{off}. (**C**) Temporal evolution of the proton pumping rate (gray) and the proton efflux rates due to passive membrane (red) leakage and transprotein backflow (blue) for the pH trace shown in (B). (**D**) Histogram of proton permeability associated with the membrane, AHA2, and AHA2^R. Respective counts were 95, 37, and 45. (**E**) Histogram of pumping rates for AHA2^R and AHA2. Respective counts were 126 and 95. (**F**) Histogram of t_{on} for AHA2^R and AHA2. Respective counts were 241 and 134. The bar at >1200 s shows the number of traces that did not switch in the duration of the experiment. (**G**) Histogram of t_{off} for AHA2^R and AHA2. Respective counts were 69 and 39. For AHA2^R and AHA2, respectively, the number of independent experiments was 3 and 2 and the number of individual proteoliposomes analyzed was 126 and 95.

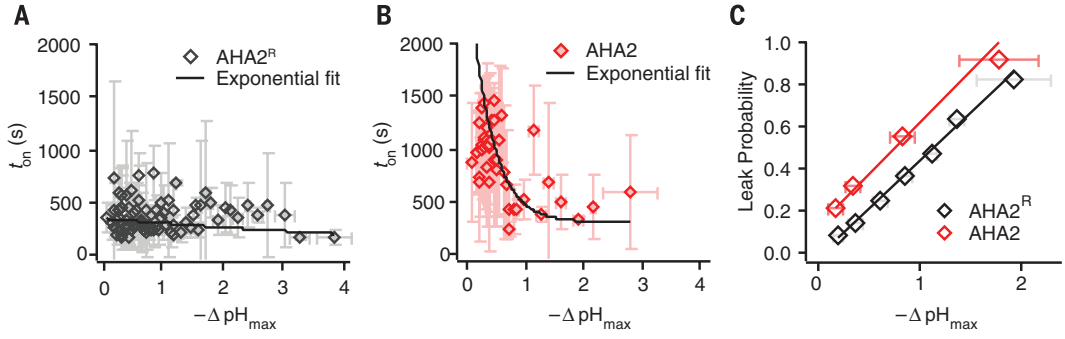

Fig. 4. Regulation of proton pumping by pH gradients. (**A** and **B**) Relation between t_{on} and the maximal pH gradient for AHA2^R and AHA2, respectively. Each data point represents the average of three consecutive values. Error bars represent corresponding standard deviations. The decay constants from the error-weighted exponential fits to the data are 6.9 ± 2.0 s and 0.4 ± 0.1 s for (A) and (B), respectively, where uncertainties represent 95% confidence intervals from the fits. (**C**) Probability of observing a transprotein leak as a function of pH gradient. For AHA2^R and AHA2, data were binned with 0.25 and 0.5 pH units; the number of independent experiments and individual proteoliposomes analyzed was the same as in Fig. 3. Spearman's rank order correlation coefficients ρ (126) = 0.40, $P = 10^{-4}$, and ρ (95) = 0.30, P = 0.03 indicated a strong positive correlation between leakage probability and ΔpH_{max} for both AHA2^R and AHA2.

Next, we quantitated proton permeabilities by fitting the kinetics with the model. The average transmembrane leak P_{leak} (Fig. 3D and fig. S11) was ~7×10^{-5} cm/s, which is in line with previous measurements and estimates (*26*), and the average transprotein leak P_{AHA2} had a similar value (~46×10^{-5} cm/s) (Fig. 3D). However, when normalized for surface area, the transprotein proton current was greater than the transmembrane by a factor of ~10^4.

The inhibitory R domain of AHA2 has been shown to reduce the net macroscopic proton transport rate by ~twofold (*10*, *11*). In order to elucidate the mechanisms underlying this regulation, we characterized the activity of the proton pump with and without the R domain. Counterintuitively, the autoinhibitory R domain increased the total time the transporter spent in the active state, both by increasing t_{on} ~threefold (from 337 to 951 s, $P = 10^{-19}$) and by decreasing t_{off} ~0.5-fold (from 121 to 65 s, $P = 0.05$) (decay constants of exponential fits to the distributions in Fig. 3, F and G; unless otherwise stated, P is a Kolmogorov-Smirnoff test of statistical similarity between two distributions). Thus, the probability of finding the pump in an active state $P_{on} = t_{on}/(t_{on} + t_{off})$ increased ~200% for AHA2 (from 0.35 ± 0.05 to 0.76 ± 0.06). Importantly, 100% of $AHA2^R$ and ~60% of AHA2 molecules switched on/off during our observation period, highlighting the fact that functional dynamics is a dominant property of this system (Fig. 3F). The R domain also had a pronounced effect on the overall intrinsic transport rates of the pump, which were reduced by ~10-fold as compared to $AHA2^R$ (from 928 to 85 protons/s, average values, $P = 10^{-20}$) (Fig. 3E). In addition, the R domain promoted an overall decrease in the transprotein leak (~1.4-fold, $P = 0.005$) (Fig. 3D).

The activity of the pump was also regulated by the pH gradients established across the membrane during proton pumping. Increasing ΔpH_{max} decreased by >twofold the lifetime of the active state, but only for the wild type (Fig. 4A, B). This regulation seems to be transmitted allosterically across the bilayer, because the R domain of AHA2 is facing the vesicle exterior, where the pH remains constant. In addition, traces with larger ΔpH_{max} had a dramatic eightfold increase (from 0.1 to 0.8) in the probability of a transprotein leak for both forms of AHA2 (Fig. 4C). Thus, regulation by pH gradients can manifest through two mechanistically distinct processes that reduce the net average proton transport: reduction of the pumping lifetime and increase of the probability of a transprotein leak, whereby only the former is encoded in the R domain.

Our observations of proton transport and leakage dynamics at the single-molecule level also provide critical insights into the ATP/H^+ stoichiometry (*27*, *28*). Ensemble average experiments have reported that the buildup of pH gradients can in general alter the stoichiometry of transport and therefore pumping rates (*27*, *28*). Contrary to expectation, we found that the intrinsic (single-molecule) pumping rate remained constant for gradients as large as 2 pH units (Fig. 3, B and C, and fig. S12C). As discussed above, pH gradients did reduce the net proton transport, but primarily by increasing the probability of a downhill transprotein leak (Fig. 4C). However, because the transprotein leak takes place once the pump has switched to the inactive state (Fig. 3C, S9), it does not affect the actual stoichiometry of active transport. In contrast, the R domain reduced the intrinsic pumping rates by ~10-fold (Fig. 4E). Because the R domain does not significantly affect the ensemble average ATPase activity (*10*, *29*), our measurements suggest that the R domain can reduce the stoichiometry of active transport by a factor of ~10 (or 20 if we correct for the change in P_{on}) (*11*). Finally, we note that our measurements of proton transport were integrated over thousands of Post-Albers catalytic cycles per second per single molecule. A better mechanistic understanding of these processes would ultimately require direct measurement of the stoichiometry at the level of single turnover cycles or careful molecular simulations.

We have developed a technique to observe, in a highly parallel manner, uphill substrate transport mediated by single transporter molecules into single nanoscopic lipid vesicles. Our measurements revealed the existence and the dynamics of several distinct functional states (active, inactive, and leaky) that together defined the activity and regulation of the proton pump, and that, we anticipate, underlie the operation of many other primary and secondary active transporters. The assays introduced here render these processes accessible to direct experimental observation.

REFERENCES AND NOTES

1. F. Ashcroft, D. Gadsby, C. Miller, *Philos. Trans. R. Soc. London Ser. B* **364**, 145–147 (2009).
2. E. Neher, B. Sakmann, *Nature* **260**, 799–802 (1976).
3. J. P. Morth *et al.*, *Nat. Rev. Mol. Cell Biol.* **12**, 60–70 (2011).
4. L. J. DeFelice, T. Goswami, *Annu. Rev. Physiol.* **69**, 87–112 (2007).
5. R. Peters, *Annu. Rev. Biophys. Biomol. Struct.* **32**, 47–67 (2003).
6. A. Tonnesen, S. M. Christensen, V. Tkach, D. Stamou, *Biophys. J.* **106**, 201–209 (2014).
7. R. Watanabe *et al.*, *Nat. Commun.* **5**, 4519 (2014).
8. M. Li *et al.*, *J. Am. Chem. Soc.* **137**, 16055–16063 (2015).
9. B. P. Pedersen, M. J. Buch-Pedersen, J. P. Morth, M. G. Palmgren, P. Nissen, *Nature* **450**, 1111–1114 (2007).
10. M. G. Palmgren, C. Larsson, M. Sommarin, *J. Biol. Chem.* **265**, 13423–13426 (1990).
11. M. G. Palmgren, P. Nissen, *Annu. Rev. Biophys.* **40**, 243–266 (2011).
12. See materials and methods and supplementary information on *Science* Online
13. S. Mathiasen *et al.*, *Nat. Methods* **11**, 931–934 (2014).
14. P. M. Bendix, M. S. Pedersen, D. Stamou, *Proc. Natl. Acad. Sci. U.S.A.* **106**, 12341–12346 (2009).
15. D. Stamou, C. Duschl, E. Delamarche, H. Vogel, *Angew. Chem. Int. Ed. Engl.* **42**, 5580–5583 (2003).
16. G. C. Kemmer *et al.*, *Analyst* **140**, 6313–6320 (2015).
17. L. Iversen *et al.*, *Science* **345**, 50–54 (2014).
18. M. J. Comstock *et al.*, *Science* **348**, 352–354 (2015).
19. T. Yanagida, Y. Ishii, Eds., *Single Molecule Dynamics in Life Science* (Wiley-VCH, Weinheim, Germany, 2009).
20. X. S. Xie, in *Single Molecule Spectroscopy in Chemistry, Physics and Biology*, A. Graslund, R. Rigler, J. Widengren, Eds. (Springer-Verlag Berlin, 2010), vol. 96, pp. 435–448.
21. N. Akyuz *et al.*, *Nature* **518**, 68 (2015).
22. C. E. Aitken, J. D. Puglisi, *Nat. Struct. Mol. Biol.* **17**, 793–800 (2010).
23. G.-W. Li, E. Oh, J. S. Weissman, *Nature* **484**, 538–541 (2012).
24. A. R. Subramaniam, B. M. Zid, E. K. O'Shea, *Cell* **159**, 1200–1211 (2014).
25. B. Sakmann, E. Neher, Eds., *Single-Channel Recording* (Springer, New York, ed. 2, 2009).
26. M. Grabe, G. Oster, *J. Gen. Physiol.* **117**, 329–344 (2001).
27. M. C. Berman, *Biochim. Biophys. Acta* **1513**, 95–121 (2001).
28. N. Nelson, A. Sacher, H. Nelson, *Nat. Rev. Mol. Cell Biol.* **3**, 876–881 (2002).
29. M. G. Palmgren, M. Sommarin, R. Serrano, C. Larsson, *J. Biol. Chem.* **266**, 20470–20475 (1991).

ACKNOWLEDGMENTS

This work was supported by the Lundbeck Foundation (Center of Excellence Biomembranes in Nanomedicine); the Danish Councils for Independent (grant number 1323-00297) and Strategic Research; the Danish National Research Foundation (Center of Excellence PUMPKIN, grant number DNRF85); the University of Copenhagen programs of excellence Single Molecule Nanoscience, BioScaRT, and UNIK-Synthetic Biology; and the National Institutes of Health (grant number R21-GM100224). We are grateful to M. G. Palmgren, J. Mindell, and P. Nissen for stimulating discussions and comments on the manuscript; M. G. Palmgren for generously providing plasmids; U. Gether for instrumentation; and A.-M. Bjerg Petersen for excellent technical assistance. D.S. conceived the strategy and was responsible for the overall project supervision. B.H.J. performed cloning. G.C.K., B.H.J., and I.L.J. expressed, purified, and reconstituted $AHA2^R$ and AHA2 and performed macroscopic measurements and data analysis under the supervision of T.G.P. T.G.P. synthesized and G.C.K purified pHrodo-PE; J.S. performed and analyzed mass spectrometry experiments of pHrodo-PE. S.M.C. wrote software for analyzing time-lapse sequences of single vesicles. S.V. designed, performed, and analyzed most single-vesicle experiments, with help from M.P.M and G.G., under the supervision of S.M.C. and D.S.. C.L., A.L.C., and N.S.H. contributed with preliminary single-vesicle acidification measurements. M.G. contributed the model of vesicle acidification. D.S. wrote the manuscript, and S.V., G.G., M.P.M., B.H.J., G.C.K., I.L.J., and T.G.P. helped prepare figures and supplementary materials. All authors discussed the results and commented on the manuscript.

SUPPLEMENTARY MATERIALS

www.sciencemag.org/content/351/6280/1469/suppl/DC1
Materials and Methods
Supplementary Text
Figs. S1 to S12
Tables S1 and S2
References (*30*–*47*)

15 October 2015; accepted 23 February 2016
10.1126/science.aad6429

Direct observation of proton pumping by a eukaryotic P-type ATPase

Salome Veshaguri, Sune M. Christensen, Gerdi C. Kemmer, Garima Ghale, Mads P. Møller, Christina Lohr, Andreas L. Christensen, Bo H. Justesen, Ida L. Jørgensen, Jürgen Schiller, Nikos S. Hatzakis, Michael Grabe, Thomas Günther Pomorski and Dimitrios Stamou

Science **351** (6280), 1469-1473.
DOI: 10.1126/science.aad6429

A proton pump in action

P-type adenosine triphosphatases (ATPases) use the energy from ATP hydrolysis to pump cations across biological membranes. The electrochemical gradients that are generated control many essential cellular processes. Veshaguri *et al.* incorporated a plant proton pump into vesicles and monitored the dynamics of single pumps. Pumping was stochastically interrupted by long-lived inactive or leaky states. The work reveals how these proton pumps are regulated by a protein domain and by pH gradients.

Science, this issue p. 1469